JOURNAL OF SPACECRAFT AND ROCKETS
Vol. 35, No. 5, September–October 1998

Effect of Magnetic Field on the Structure of High-Speed Flows

Justin Augustinus,* Klaus A. Hoffmann,† and Shigeki Harada*
Wichita State University, Wichita, Kansas 67260-0044

The eight-wave ideal magnetohydrodynamics(MHD) equations are extended to two dimensions and applied to a blunt two-dimensional body at hypersonic speeds. Several developments are reported on. 1) The two-dimensional governing equations of ideal MHD equations are derived in the generalized coordinate system. 2) A set of eigenvectors associated with the system of equations is developed for the implementation of the numerical scheme. 3) A solution is obtained for a blunt two-dimensional body at hypersonic speed. 4) The effect of the magnetic field on the flowfield structure is investigated. When the external magnetic field is activated, the solution indicates an increase in shock standoff distance and a corresponding decrease in total pressure. Furthermore, a contact discontinuity around the nose region is generated, and the flow loses symmetricity along the body axis. The numerical scheme used is the modified Runge–Kutta scheme with the total variation diminishing model augmented as a postprocessor approach at each time level.

Nomenclature

B_x, B_y, B_z	= magnetic field components in the x, y, and z directions
c_s	= speed of sound
$\boldsymbol{E}$, $\boldsymbol{F}$	= flux vector components in the x and y directions
e_t	= total energy per unit mass
J	= Jacobian of transformation
p	= pressure
$\boldsymbol{Q}$	= field vector
U, V	= contravarient velocity components
u, v, w	= velocity components in the x, y, and z directions
v_{ax}, v_{ay}	= Alfvén wave velocity in the x and y directions
x, y	= Cartesian coordinates
γ	= ratio of specific heats
λ	= eigenvalue
ξ, η	= generalized coordinates
ρ	= density
$\boldsymbol{\Phi}_\xi$, $\boldsymbol{\Phi}_\eta$	= flux limiter function vectors associated with A and B

Subscripts

a	= Alfvén wave
f	= fast wave
s	= slow wave

I. Introduction

SEVERAL interesting and important problems arise in astrophysics, solar, magnetospheric, thermonuclear, electrical, and aerospace engineering that can be simulated by the solution of magnetohydrodynamic (MHD) equations. For instance, a space vehicle traveling at hypersonic speed upon re-entry will dissociate and ionize the flow around it due to high temperatures created by the bow shock up front. The magnetized plasma can create a magnetic field, which must be considered in the design of the heat shield, flight controls, and communication apparatus. The effect of the magnetic field on the flowfield around a Mars return aerobrake was analyzed by Palmer.[1] Similarly, in solar activities MHD equations have been used to simulate the interaction of an expanding cometary atmosphere with the solar wind to capture the bow shock and contact surface properties.[2]

The governing equations of MHD characterize the flow of electrically conducting fluid in the presence of a magnetic field. They represent coupling of fluid dynamic equations and Maxwell's equation of electrodynamics. By neglecting dissipation terms and hence assuming the flow to be non-heat-conducting inviscid, and with no electrostatic force, displacement current, and resistivity, the MHD equations reduce to the ideal MHD equations.

Unlike the Euler equations, the ideal MHD equations are not a strictly hyperbolic system because the eigenvalues may coincide, and furthermore they are nonconvex, which means that some of their characteristic fields are neither linearly degenerate nor genuinely nonlinear. For instance, one can have a compound wave that consists of a shock and attached to it a rarefaction wave of the same family. Despite all of the complexity of the ideal MHD equations, various numerical techniques have been successful in solving these equations for both one-dimensional and multidimensional problems.

In recent years the higher-order Godunov scheme seems to have gained much popularity. Zachary and Colella[3] solved the one-dimensional ideal MHD equations using a high-order Godunov scheme. Their scheme[3] is based on the methods discussed by Bell et al.,[4] with appropriate extension and generalization to MHD equations. Zachary and Colella[3] extended their application to Brio and Wu's[5] shock tube problem, and their results were in good agreement with calculations of Brio and Wu.[5] Dai and Woodward[6] extended the piecewise parabolic method (PPM) to multidimensional ideal MHD equations based on an iterative nonlinear Riemann solver. Later Dai and Woodward[7] developed an approximate Riemann solver for use in a high-order Godunov scheme based on characteristic formulation for the one-dimensional MHD problem. Results were compared to the PPM formulation[6] for both the Euler and the ideal MHD equations and to the available exact solutions of Riemann problems for ideal MHD equations. The robustness of the Dai and Woodward[7] scheme was demonstrated through numerical examples involving more than one strong shock at the same time. Their scheme offered the principle advantages of high-order Godunov schemes: robust operation in the presence of strong waves, thin shock fronts, thin contact, and slip surface discontinuities. Recently Dai and Woodward[8] introduced an iterative implicit–explicit hybrid scheme for hyperbolic systems of conservation laws. This new scheme is of Godunov type in both explicit and implicit regimes, it is in a strict conservation form, and it is accurate to the second order in both space and time for all Courant numbers.

Recently, a class of schemes known as total variation diminishing (TVD) has been introduced. These schemes ensure that the TVD of the flow variables does not increase with time; thus, no spurious numerical oscillations are generated. The solution can be higher order in the smooth parts of the flowfield, but the scheme switches to first order at the extrema. The TVD models commonly used are the non-MUSCL TVD models of Harten, Yee, and Roe. The investigation by Reddy and Papadakis[9] shows that these TVD models are able to capture discontinuities more accurately than nonlinear dissipation models. Another advantage of TVD models over the nonlinear

Received Sept. 2, 1997; revision received April 25, 1998; accepted for publication April 28, 1998.

*Research Assistant, Department of Aerospace Engineering. Student Member AIAA.

†Associate Professor, Department of Aerospace Engineering. Associate Fellow AIAA.

dissipation models is that user-specified input is no longer required. However, these advantages of TVD models are accompanied by a disadvantage, i.e., they require smaller time steps to yield to a stable solution and, hence, they typically require more computational time. There is a price to be paid for accuracy. It is also noted that TVD formulations require both left and right eigenvectors and eigenvalues of the Jacobian matrices, which require additional effort in development of the scheme.

Quite recently the monotonicity of the TVD property of the TVD schemes has been proven for ideal MHD equations. Barmin et al.[10] used the upwind and symmetric TVD schemes to investigate the possibility of appearances of nonevolutionary solutions during the shock-capturing modeling of ideal MHD flows. To avoid the calculation of right and inverse right eigenvectors of the system in each grid point in their TVD scheme, the spectral radius of the Jacobian matrix is used instead. Toth and Odstrcil[11] made comparisons with two versions of flux-corrected transport and two versions of TVD schemes for several one-dimensional and two-dimensional hydrodynamic and MHD problems.

The extension of one-dimensional, seven-wave ideal MHD equations to multidimensions is not straightforward for a Riemann solver that would be based on the eigensystem of the Jacobian matrix. This is because the Jacobian matrix is singular; the fifth row of the matrix is zero, leading to a zero eigenvalue. The zero eigenvalue indicates clearly a nonphysical system. For a physical system, the eigenvalues should appear either singly as the x component of the flow speed u or in pairs symmetric about u. Powell et al.[12] have developed a new set of governing ideal MHD equations that can be used to solve multidimensional problems and applied it to an astrophysics problem. In the new set of governing equations, Powell et al.[12] introduced a new eigenvalue u (an eighth wave) that is called the magnetic divergence wave. The new eight-wave system has a source term that is proportional to $\nabla \cdot \boldsymbol{B}$. It is noted that the resulting system is no longer in conservative form, and furthermore, the added source term is zero ($\nabla \cdot \boldsymbol{B} = 0$), an additional condition that must be satisfied by the ideal MHD equations. It has been previously noted[13] that solving the momentum equation in nonconservative form can remove instabilities related to nonzero $\nabla \cdot \boldsymbol{B}$. However, Dai and Woodward[6] did use the seven-wave system of equations to solve a two-dimensional system. Their scheme is built on the dimensional splitting method originally suggested by Strang.[14] In each time step of the two-dimensional problem, it is split into two one-dimensional passes in which derivatives in the other direction are set to zero. Each row in the grid is treated as if it was an independent one-dimensional problem. After all of the rows in one direction are applied by the one-dimensional functioning code, another pass in the other direction is made. These x and y passes compose only the first half-time step, whereas in the other half the scheme carries out the y pass first followed by the x pass.

The aim of the present work is to develop a new numerical scheme for the ideal MHD equations. The modified Runge–Kutta (R–K) integration scheme has been chosen as the basic numerical scheme. To stabilize the modified R–K scheme, the non-MUSCL TVD flux limiters are added in a postprocessor approach. The postprocessor approach can be easily applied to many single- and multistep-explicit schemes by adding an extra step to the original dissipation-free scheme. This approach becomes very convenient because no modification to the existing numerical scheme is necessary. For the one-dimensional case, numerical experiments have been conducted for both the seven-wave and eight-wave systems with various TVD limiters.[15,16] A new set of right and left eigenvectors in the generalized coordinates has also been developed in this work inasmuch as its usage is necessary for the implementation of the TVD model in the generalized coordinate system. The numerical procedure has been extended to two dimensions, and the effects of the magnetic field for a blunt body traveling at hypersonic speed are presented.

II. Governing Equations

The ideal magnetohydrodynamics equations in two dimensions are given by

$$\frac{\partial \boldsymbol{Q}}{\partial t} + \frac{\partial \boldsymbol{E}}{\partial x} + \frac{\partial \boldsymbol{F}}{\partial y} = \boldsymbol{H} \tag{1}$$

where the vector of conservative variables $\boldsymbol{Q}$ and the flux vectors $\boldsymbol{E}$, $\boldsymbol{F}$, and $\boldsymbol{H}$ are

$$\boldsymbol{Q} = [\rho, \rho u, \rho v, \rho w, B_x, B_y, B_z, \rho e_t]^T \tag{2}$$

$$\boldsymbol{E} = \begin{bmatrix} \rho u \\ \rho u^2 + p + \dfrac{\left(-B_x^2 + B_y^2 + B_z^2\right)}{8\pi} \\ \rho uv - \dfrac{B_x B_y}{4\pi} \\ \rho uw - \dfrac{B_x B_z}{4\pi} \\ 0 \\ uB_y - vB_x \\ uB_z - wB_x \\ \left[\rho e_t + p + \dfrac{\left(B_x^2 + B_y^2 + B_z^2\right)}{8\pi}\right] u - \dfrac{B_x}{4\pi}(uB_x + vB_y + wB_z) \end{bmatrix} \tag{3}$$

$$\boldsymbol{F} = \begin{bmatrix} \rho v \\ \rho vu - \dfrac{B_y B_x}{4\pi} \\ \rho v^2 + p + \dfrac{\left(B_x^2 - B_y^2 + B_z^2\right)}{8\pi} \\ \rho vw - \dfrac{B_y B_z}{4\pi} \\ vB_x - uB_y \\ 0 \\ vB_z - wB_y \\ \left[\rho e_t + p + \dfrac{\left(B_x^2 + B_y^2 + B_z^2\right)}{8\pi}\right] v - \dfrac{B_y}{4\pi}(uB_x + vB_y + wB_z) \end{bmatrix} \tag{4}$$

$$\boldsymbol{H} = \boldsymbol{H}_M \left(\frac{\partial B_x}{\partial x} + \frac{\partial B_y}{\partial y} \right) \tag{5}$$

$$\boldsymbol{H}_M = -\left[0, \frac{B_x}{4\pi}, \frac{B_y}{4\pi}, \frac{B_z}{4\pi}, u, v, w, \frac{uB_x + vB_y + wB_z}{4\pi}\right]^T \tag{6}$$

The MHD equation given by Eq. (1) is transformed to a computational space and expressed as

$$\frac{\partial \bar{\boldsymbol{Q}}}{\partial t} + \frac{\partial \bar{\boldsymbol{E}}}{\partial \xi} + \frac{\partial \bar{\boldsymbol{F}}}{\partial \eta} = \bar{\boldsymbol{H}} \tag{7}$$

where

$$\bar{\boldsymbol{Q}} = \frac{\boldsymbol{Q}}{J}, \qquad \bar{\boldsymbol{E}} = \frac{\xi_x \boldsymbol{E} + \xi_y \boldsymbol{F}}{J}, \qquad \bar{\boldsymbol{F}} = \frac{\eta_x \boldsymbol{E} + \eta_y \boldsymbol{F}}{J}$$

$$\bar{B}_x = \frac{\xi_x B_x + \xi_y B_y}{J}, \qquad \bar{B}_y = \frac{\eta_x B_x + \eta_y B_y}{J}$$

$$\bar{\boldsymbol{H}} = \boldsymbol{H}_M \left(\frac{\partial \bar{B}_x}{\partial \xi} + \frac{\partial \bar{B}_y}{\partial \eta} \right)$$

and $\boldsymbol{H}_M$ is given in Eq. (6).

The flux vectors $\bar{E}$ and $\bar{F}$ in Eq. (7) can be written in terms of vector $\bar{Q}$ by defining the Jacobian matrices $\bar{A}$ and $\bar{B}$ and subsequently rewriting Eq. (7) as

$$\frac{\partial \bar{Q}}{\partial t} + \bar{A}\frac{\partial \bar{Q}}{\partial \xi} + \bar{B}\frac{\partial \bar{Q}}{\partial \eta} = 0 \tag{8}$$

where

$$\bar{A} = \frac{\partial \bar{E}}{\partial \bar{Q}} - H_M \frac{\partial \bar{B}_x}{\partial \bar{Q}} = (\xi_x A + \xi_x B) \tag{9}$$

and

$$\bar{B} = \frac{\partial \bar{F}}{\partial \bar{Q}} - H_M \frac{\partial \bar{B}_y}{\partial \bar{Q}} = (\eta_x A + \eta_y B) \tag{10}$$

The Jacobian matrices A and B are defined as

$$A = \frac{\partial E}{\partial Q} - H_M \frac{\partial B_x}{\partial Q}, \qquad B = \frac{\partial F}{\partial Q} - H_M \frac{\partial B_y}{\partial Q}$$

III. Eigenvalues and Eigenvectors

The numerical scheme used to solve Eq. (8) requires the eigenvalues and eigenvectors of the Jacobian matrices. In this section both the eigenvalues and eigenvectors are provided. The eigenvalues of the Jacobian $\bar{A}$ matrix are derived to be

$$\lambda_{0\xi} = \xi_x u + \xi_y v \tag{11a}$$

$$\lambda_{a\xi\pm} = \xi_x(u \pm v_{ax}) + \xi_y(v \pm v_{ay}) \tag{11b}$$

$$\lambda_{f\xi\pm} = \xi_x u + \xi_y v \pm v_{f\xi} \tag{11c}$$

$$\lambda_{s\xi\pm} = \xi_x u + \xi_y v \pm v_{s\xi} \tag{11d}$$

$$\lambda_{d\xi} = \xi_x u + \xi_y v \tag{11e}$$

where

$$v_{f\xi}^2 = \tfrac{1}{4}\left[2\left(v_a^2 + c_s^2\right)\left(\xi_x^2 + \xi_y^2\right) + z_\xi\right]$$

$$v_{s\xi}^2 = \tfrac{1}{4}\left[2\left(v_a^2 + c_s^2\right)\left(\xi_x^2 + \xi_y^2\right) - z_\xi\right]$$

$$z_\xi = 2\sqrt{\xi_x^2 + \xi_y^2}\sqrt{\left(v_a^2 + c_s^2\right)^2\left(\xi_x^2 + \xi_y^2\right) - \frac{(\xi_x B_x + \xi_y B_y)^2 \gamma p}{\rho^2 \pi}}$$

and v_{ax}, v_{ay}, c_s, and v_a are defined as

$$v_{ax}^2 = \frac{B_x^2}{4\pi\rho}, \qquad v_{ay}^2 = \frac{B_y^2}{4\pi\rho}, \qquad c_s^2 = \frac{\gamma p}{\rho}$$

$$v_a^2 = \frac{\left(B_x^2 + B_y^2 + B_z^2\right)}{4\pi\rho}$$

The diagonal eigenvalue matrix

$$D_\xi = L_\xi \bar{A} R_\xi \tag{12}$$

then becomes

$$D_\xi = \begin{bmatrix} \lambda_{0\xi} & 0 & 0 & 0 & 0 & 0 & 0 & 0 \\ 0 & \lambda_{a\xi+} & 0 & 0 & 0 & 0 & 0 & 0 \\ 0 & 0 & \lambda_{a\xi-} & 0 & 0 & 0 & 0 & 0 \\ 0 & 0 & 0 & \lambda_{f\xi+} & 0 & 0 & 0 & 0 \\ 0 & 0 & 0 & 0 & \lambda_{f\xi-} & 0 & 0 & 0 \\ 0 & 0 & 0 & 0 & 0 & \lambda_{s\xi+} & 0 & 0 \\ 0 & 0 & 0 & 0 & 0 & 0 & \lambda_{s\xi-} & 0 \\ 0 & 0 & 0 & 0 & 0 & 0 & 0 & \lambda_{d\xi} \end{bmatrix}$$

where the right and left eigenvectors are

$$R_\xi = \left[\boldsymbol{r}_0, \boldsymbol{r}_{+v_{a\xi}}, \boldsymbol{r}_{-v_{a\xi}}, \boldsymbol{r}_{+v_{f\xi}}, \boldsymbol{r}_{-v_{f\xi}}, \boldsymbol{r}_{+v_{s\xi}}, \boldsymbol{r}_{-v_{s\xi}}, \boldsymbol{r}_{d\xi}\right]$$

$$L_\xi = \left[\boldsymbol{l}_0, \boldsymbol{l}_{+v_{a\xi}}, \boldsymbol{l}_{-v_{a\xi}}, \boldsymbol{l}_{+v_{f\xi}}, \boldsymbol{l}_{-v_{f\xi}}, \boldsymbol{l}_{+v_{s\xi}}, \boldsymbol{l}_{-v_{s\xi}}, \boldsymbol{l}_{d\xi}\right]^T$$

Similarly, the eigenvalues of the flux Jacobian $\bar{B}$ matrix are

$$\lambda_{0\eta} = \eta_x u + \eta_y v \tag{13a}$$

$$\lambda_{a\eta\pm} = \eta_x(u \pm v_{ax}) + \eta_y(v \pm v_{ay}) \tag{13b}$$

$$\lambda_{f\eta\pm} = \eta_x u + \eta_y v \pm v_{f\eta} \tag{13c}$$

$$\lambda_{s\eta\pm} = \eta_x u + \eta_y v \pm v_{s\eta} \tag{13d}$$

$$\lambda_{d\eta} = \eta_x u + \eta_y v \tag{13e}$$

where

$$v_{f\eta}^2 = \tfrac{1}{4}\left[2\left(v_a^2 + c_s^2\right)\left(\eta_x^2 + \eta_y^2\right) + z_\eta\right]$$

$$v_{s\eta}^2 = \tfrac{1}{4}\left[2\left(v_a^2 + c_s^2\right)\left(\eta_x^2 + \eta_y^2\right) - z_\eta\right]$$

$$z_\eta = 2\sqrt{\eta_x^2 + \eta_y^2}\sqrt{\left(v_a^2 + c_s^2\right)\left(\eta_x^2 + \eta_y^2\right) - \frac{(\eta_x B_x + \eta_y B_y)^2 \gamma p}{\rho^2 \pi}}$$

and v_{ax}, v_{ay}, c_s, and v_a are as already defined.

The diagonal eigenvalue matrix

$$D_\eta = L_\eta \bar{B} R_\eta \tag{14}$$

then becomes

$$D_\eta = \begin{bmatrix} \lambda_{0\eta} & 0 & 0 & 0 & 0 & 0 & 0 & 0 \\ 0 & \lambda_{a\eta+} & 0 & 0 & 0 & 0 & 0 & 0 \\ 0 & 0 & \lambda_{a\eta-} & 0 & 0 & 0 & 0 & 0 \\ 0 & 0 & 0 & \lambda_{f\eta+} & 0 & 0 & 0 & 0 \\ 0 & 0 & 0 & 0 & \lambda_{f\eta-} & 0 & 0 & 0 \\ 0 & 0 & 0 & 0 & 0 & \lambda_{s\eta+} & 0 & 0 \\ 0 & 0 & 0 & 0 & 0 & 0 & \lambda_{s\eta-} & 0 \\ 0 & 0 & 0 & 0 & 0 & 0 & 0 & \lambda_{d\eta} \end{bmatrix}$$

where

$$R_\eta = \left[\boldsymbol{r}_0, \boldsymbol{r}_{+v_{a\eta}}, \boldsymbol{r}_{-v_{a\eta}}, \boldsymbol{r}_{+v_{f\eta}}, \boldsymbol{r}_{-v_{f\eta}}, \boldsymbol{r}_{+v_{s\eta}}, \boldsymbol{r}_{-v_{s\eta}}, \boldsymbol{r}_{d\eta}\right]$$

$$L_\eta = \left[\boldsymbol{l}_0, \boldsymbol{l}_{+v_{a\eta}}, \boldsymbol{l}_{-v_{a\eta}}, \boldsymbol{l}_{+v_{f\eta}}, \boldsymbol{l}_{-v_{f\eta}}, \boldsymbol{l}_{+v_{s\eta}}, \boldsymbol{l}_{-v_{s\eta}}, \boldsymbol{l}_{d\eta}\right]^T$$

IV. Numerical Schemes

The aim of the present work is to develop a numerical scheme for the ideal MHD equations based on the TVD formulation. The new scheme is composed of the modified R–K integration scheme augmented with TVD flux limiters in a postprocessor approach.

Harada et al.[15] developed a numerical scheme based on a modified R–K scheme with several TVD models to solve the seven-wave system for the magnetic shock tube. The upwind TVD schemes of Harten–Yee (H–Y) and Roe–Sweby (R–S) and the symmetric TVD of Davis–Yee (D–Y) along with several limiters within each category were investigated. The procedure was extended to the eight-wave system by Augustinus et al.[16] Several investigations have identified the accuracy of solutions obtained by each limiter.[15,16] The numerical procedures developed in Refs. 15 and 16 are extended to two-dimensional problems in this paper.

To extend the scheme to the ideal MHD equations in the generalized coordinates, a complete set of right and inverse right eigenvectors had to be formulated.

The modified R–K scheme for the two-dimensional ideal MHD equations in the generalized coordinate system is

$$\bar{Q}_{i,j}^{(1)} = \bar{Q}_{i,j}^{n} - (\Delta t/4)(L\bar{Q}^{n})_{i,j} \tag{15a}$$

$$\bar{Q}_{i,j}^{(2)} = \bar{Q}_{i,j}^{n} - (\Delta t/3)\left(L\bar{Q}^{(1)}\right)_{i,j} \tag{15b}$$

$$\bar{Q}_{i,j}^{(3)} = \bar{Q}_{i,j}^{n} - (\Delta t/2)\left(L\bar{Q}^{(2)}\right)_{i,j} \tag{15c}$$

$$\bar{Q}_{i,j}^{n+1} = \bar{Q}_{i,j}^{n} - \Delta t\left(L\bar{Q}^{(3)}\right)_{i,j} \tag{15d}$$

where

$$(L\bar{Q})_{i,j} = \frac{(\bar{E}_{i+1,j} - \bar{E}_{i-1,j})}{2\Delta\xi} + \frac{(\bar{F}_{i,j+1} - \bar{F}_{i,j-1})}{2\Delta\eta} - \bar{H}_{i,j}$$

TVD

The modified R–K scheme may become unstable when solving Riemann-like problems because it uses central differencing of the convective terms. Therefore, it is necessary to add an artificial dissipation term to stabilize the scheme. The artificial dissipation term used in this research is the TVD model.

The following is the addition of the TVD model in the generalized coordinate system:

$$\bar{Q}^{n+1}_{i,j} = \bar{Q}^{n+1}_{i,j} - \frac{\Delta t}{2\Delta\xi} \times \left[(R_\xi)_{i+\frac{1}{2},j}(\Phi_\xi)_{i+\frac{1}{2},j} - (R_\xi)_{i-\frac{1}{2},j}(\Phi_\xi)_{i-\frac{1}{2},j} \right] - \frac{\Delta t}{2\Delta\eta}\left[(R_\eta)_{i,j+\frac{1}{2}}(\Phi_\eta)_{i,j+\frac{1}{2}} - (R_\eta)_{i,j-\frac{1}{2}}(\Phi_\eta)_{i,j-\frac{1}{2}} \right] \quad (16)$$

The flux limiter function vectors Φ_ξ and Φ_η are

$$(\Phi_\xi)_{i+\frac{1}{2},j} = \left[\left(\phi^1_\xi\right)_{i+\frac{1}{2},j}, \left(\phi^2_\xi\right)_{i+\frac{1}{2},j}, \left(\phi^3_\xi\right)_{i+\frac{1}{2},j}, \ldots \right]^T \quad (17a)$$

$$(\Phi_\eta)_{i,j+\frac{1}{2}} = \left[\left(\phi^1_\eta\right)_{i,j+\frac{1}{2}}, \left(\phi^2_\eta\right)_{i,j+\frac{1}{2}}, \left(\phi^3_\eta\right)_{i,j+\frac{1}{2}}, \ldots \right]^T \quad (17b)$$

Davis–Yee Symmetric TVD Model

For the D–Y symmetric TVD model, the lth symmetric flux-limiter function is given by

$$\left(\phi^l_\xi\right)_{i+\frac{1}{2},j} = -\left\{ \frac{\Delta t}{\Delta\xi}\left[\left(\lambda^l_\xi\right)_{i+\frac{1}{2},j}\right]^2 \left(g^l_\xi\right)_{i+\frac{1}{2},j} + \varphi\left[\left(\lambda^l_\xi\right)_{i+\frac{1}{2},j}\right]\left[(\alpha^l)_{i+\frac{1}{2},j} - \left(g^l_\xi\right)_{i+\frac{1}{2},j}\right]\right\} \quad (18a)$$

$$\left(\phi^l_\eta\right)_{i,j+\frac{1}{2}} = -\left\{ \frac{\Delta t}{\Delta\eta}\left[\left(\lambda^l_\eta\right)_{i,j+\frac{1}{2}}\right]^2 \left(g^l_\eta\right)_{i,j+\frac{1}{2}} + \varphi\left[\left(\lambda^l_\eta\right)_{i,j+\frac{1}{2}}\right]\left[(\alpha^l)_{i,j+\frac{1}{2}} - \left(g^l_\eta\right)_{i,j+\frac{1}{2},j}\right]\right\} \quad (18b)$$

where $(\lambda^l_\xi)_{i+1/2,j}$ and $(\lambda^l_\eta)_{i,j+1/2}$ are the lth eigenvalues of the diagonal matrices D_ξ and D_η. The function $\varphi(z)$ is an entropy correction to z with

$$\varphi(z) = \begin{cases} |z|, & |z| \geq \delta \\ \dfrac{z^2+\delta^2}{2\delta}, & |z| < \delta \end{cases} \quad (19)$$

where $0 < \delta < 0.125$. However, in the case of steady-state calculations for a blunt body at $M_\infty > 2.5$, a modification to the δ term has to be included; otherwise nonphysical solutions are likely to occur. The proposed δ to be used with the entropy correction term is

$$\delta_{i+\frac{1}{2},j} = \bar{\delta}\left[U_{i+\frac{1}{2},j} + V_{i+\frac{1}{2},j} + (v_{f\xi})_{i+\frac{1}{2},j} + (v_{f\eta})_{i+\frac{1}{2},j} \right] \quad (20a)$$

$$\delta_{i,j+\frac{1}{2}} = \bar{\delta}\left[U_{i,j+\frac{1}{2}} + V_{i,j+\frac{1}{2}} + (v_{f\xi})_{i,j+\frac{1}{2}} + (v_{f\eta})_{i,j+\frac{1}{2}} \right] \quad (20b)$$

where

$$U = \xi_x u + \xi_y v, \qquad V = \eta_x u + \eta_y v$$

and $0.5 < \bar{\delta} < 0.7$.

Several limiters were investigated by Augustinus et al.,[16] and one limiter performed with better accuracy. Therefore, the following is selected as the limiter associated with this symmetric TVD model:

$$\left(g^l_\xi\right)_{i+\frac{1}{2},j} = \min\text{mod}\left\{ 2(\alpha^l)_{i-\frac{1}{2},j}, 2(\alpha^l)_{i+\frac{1}{2},j}, 2(\alpha^l)_{i+\frac{3}{2},j}, \frac{1}{2}\left[(\alpha^l)_{i-\frac{1}{2},j} + (\alpha^l)_{i+\frac{3}{2},j}\right]\right\} \quad (21a)$$

$$\left(g^l_\eta\right)_{i,j+\frac{1}{2}} = \min\text{mod}\left\{ 2(\alpha^l)_{i,j-\frac{1}{2}}, 2(\alpha^l)_{i,j+\frac{1}{2}}, 2(\alpha^l)_{i,j+\frac{3}{2}}, \frac{1}{2}\left[(\alpha^l)_{i,j-\frac{1}{2}} + (\alpha^l)_{i,j+\frac{3}{2}}\right]\right\} \quad (21b)$$

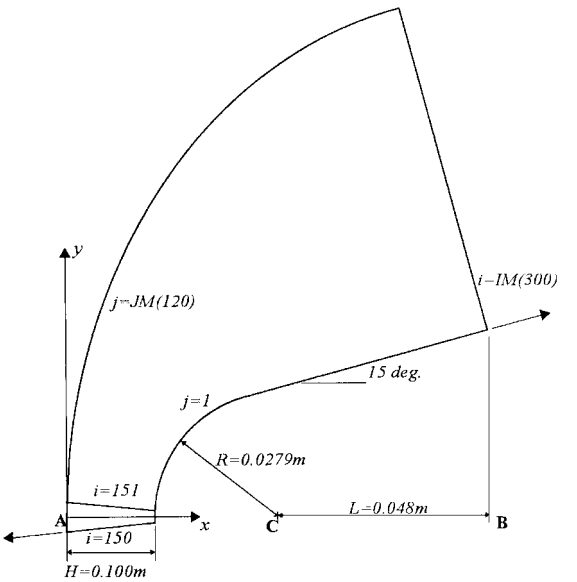

Fig. 1 Two-dimensional cylinder–wedge configuration.

where $(\alpha^l)_{i+1/2,j}$ and $(\alpha^l)_{i,j+1/2}$ are the lth elements of

$$\alpha_{i+\frac{1}{2},j} = \frac{2(L_\xi)_{i+\frac{1}{2},j}(\boldsymbol{Q}_{i+1,j} - \boldsymbol{Q}_{i,j})}{R_{i+1,j} + R_{i,j}} \quad (22a)$$

and

$$\alpha_{i,j+\frac{1}{2}} = \frac{2(L_\eta)_{i,j+\frac{1}{2}}(\boldsymbol{Q}_{i,j+1} - \boldsymbol{Q}_{i,j})}{R_{i,j+1} + R_{i,j}} \quad (22b)$$

Two-Dimensional Blunt Body

A two-dimensional, cylinder–wedge blunt body is considered for applications. A structured algebraic grid system is chosen to discretize the domain of solution. The upper half of the blunt body configuration is shown in Fig. 1. Computations are performed on a 300×120 ($IM \times JM$) grid system.

Body Configuration

The computations are performed for a two-dimensional configuration consisting of a cylindrical leading edge connected to a straight surface at 15 deg. The outer boundary of the grid is an ellipse with its center located at point B. The major and minor axes are 0.30 and 0.1759 m, respectively. The origin of the coordinate system is located at point A. The surface of the body is represented by the innermost boundary of the domain, and it is a combination of a circle of radius 0.0279 m with its center at C and a straight line inclined at 15 deg. The circle is connected to the straight line at its tangent point.

The ξ and η directions are shown in Fig. 1. Indices i and j correspond to the ξ and η locations, respectively. The blunt body surface is represented by grid line $j = 1$. The outermost boundary of the domain facing the freestream is represented by grid line $j = JM$. In the η-direction, grid line $i = 1$ and $i = IM$ correspond to the outflow boundaries. All i grid lines radiate out perpendicularly to the surface of the body. This is intentionally done so as to ease the extrapolation of fluid properties perpendicular to the surface.

Initial Conditions

A cold-start approach is used as the initial condition to this problem. In a cold-start initial solution, the freestream conditions are assumed to exist at all points of the computational domain. Thus, the freestream properties are used in the calculation of the initial time steps.

Five cases were investigated. In each case only the magnetic field strength was varied and the fluid properties were not changed. The objective is to investigate the effects of various magnetic field on the flowfield properties. The initial freestream conditions correspond to

the data of Cleary[17] and are specified as $\rho_\infty = 4.3376 \times 10^{-4}$ kg/m^3, $v_\infty = w_\infty = 0$ m/s, $p_\infty = 36.6$ N/m^2, $M_\infty = 10.6$, and $\gamma = 1.4$.

The spatial steps are $\Delta\xi = \Delta\eta = 1$, and the Courant–Friedrichs–Lewy number is 0.1.

Case 1: For this case $\boldsymbol{B} = 0$. This case was computed using the Euler equations with the same numerical scheme.

Case 2:

$$B_x = 5\sqrt{4\pi}, \qquad B_y = 0, \qquad B_z = 0$$

Case 3:

$$B_x = 0, \qquad B_y = 5\sqrt{4\pi}, \qquad B_z = 0$$

Case 4:

$$B_x = 0, \qquad B_y = 0, \qquad B_z = 5\sqrt{4\pi}$$

Case 5:

$$B_x = 0, \qquad B_y = 5\sqrt{4\pi}, \qquad B_z = 5\sqrt{4\pi}$$

Case 6:

$$B_x = 0, \qquad B_y = 4\sqrt{4\pi}, \qquad B_z = 0$$

Case 7:

$$B_x = 0, \qquad B_y = 3\sqrt{4\pi}, \qquad B_z = 0$$

Case 8:

$$B_x = 0, \qquad B_y = 2\sqrt{4\pi}, \qquad B_z = 0$$

Case 9:

$$B_x = 0, \qquad B_y = \sqrt{4\pi}, \qquad B_z = 0$$

V. Results and Discussion

To investigate the effect of the magnetic field on the flowfield, nine numerical experiments were conducted for the two-dimensional problem. Based on the results of the magnetic shock tube problem described in Refs. 15 and 16, both the D–Y symmetric TVD model and the H–Y upwind TVD model seem to yield better results than the R–S model. In general the D–Y model tends to smear both the shock and contact surface or discontinuity, whereas the H–Y model underpredicts the contact discontinuity. It is well known that a solution of a typical blunt body problem at hypersonic speeds consists of both shock and rarefaction waves. With this caveat in mind, it was decided to conduct all of the numerical experiments in this problem using the D–Y symmetric model because it is felt that the H–Y model may have the tendency to underpredict some of the rarefaction zones relating to this problem.

Case 1 represents zero magnetic field strength, and hence, $\boldsymbol{B} = 0$. In cases 2, 3, and 4 only the individual x, y, and z components of the magnetic field are introduced, respectively, with the same magnetic field strength, which is equal to $5\sqrt{(4\pi)}$. The aim of introducing these three cases is to investigate the effect of each individual magnetic field component on the flowfield. In case 5 only the y and z components are introduced, whereas the x component is set to zero. The explanation for introducing case 5 is that should a practical experiment be carried out in a wind tunnel it would be difficult to introduce the magnetic field along the flow stream compared to the tranverse directions. Also notice that the initial conditions of all of these cases satisfy the $\nabla \cdot \boldsymbol{B} = 0$ condition. In cases 6–9 the y component of the magnetic field is decreased from $4\sqrt{(4\pi)}$ to $\sqrt{(4\pi)}$.

Figures 2 and 3 represent both the pressure and density contour plots for cases 1 and 3. It is quite evident from these plots that the shock has been displaced farther away from the blunt body for case 3. Notice that the density contour plots for case 3 exhibit an additional feature adjacent to the nose of the body, which is not evident in the pressure plots. In general, this could be a contact discontinuity because across a contact discontinuity there is no change in pressure distribution. To provide an interpretation of some of the features that appear on these plots, distributions of both the flow and magnetic field properties across the solution domain are essential.

Figures 4 and 5 show the flowfield properties along the x axis, which is also the stagnation streamline for the reference case. The total density and pressure determined from the normal shock relationships for $M_1 = 10.6$ are also presented in Figs. 4 and 5, respectively. These values compare well with the computed values at $j = 1$

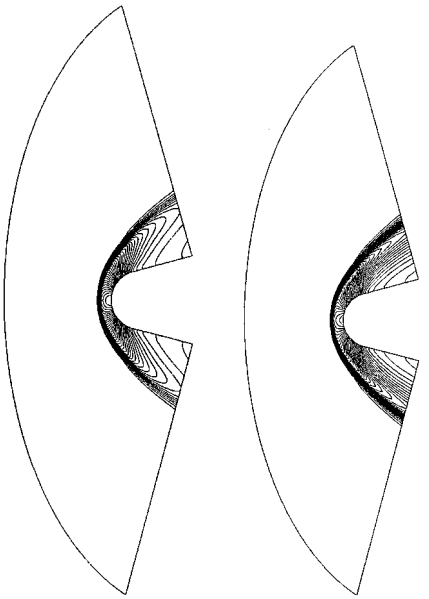

a) Pressure b) Density

Fig. 2 Case 1 contour plots.

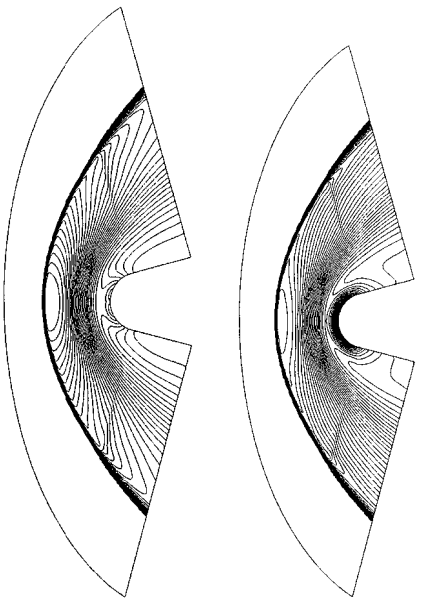

a) Pressure b) Density

Fig. 3 Case 3 contour plots.

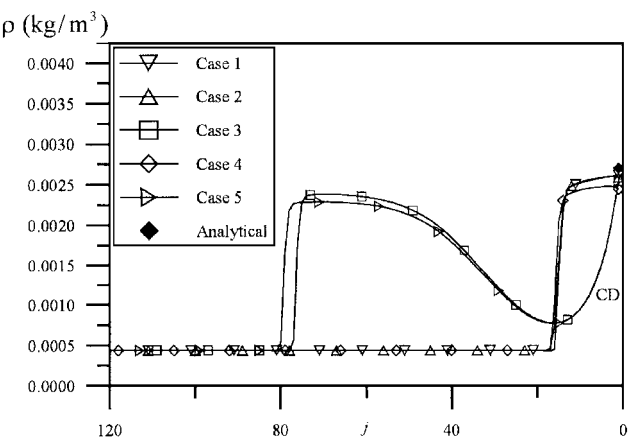

Fig. 4 Computed density distributions at $y = 0$ m.

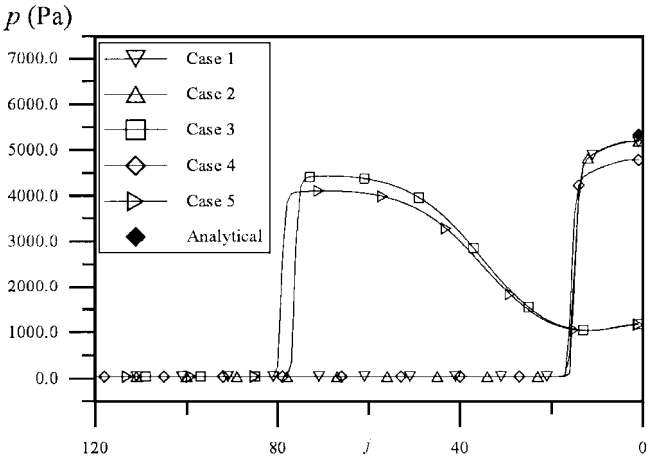

Fig. 5 Computed pressure distributions at $y = 0$ m.

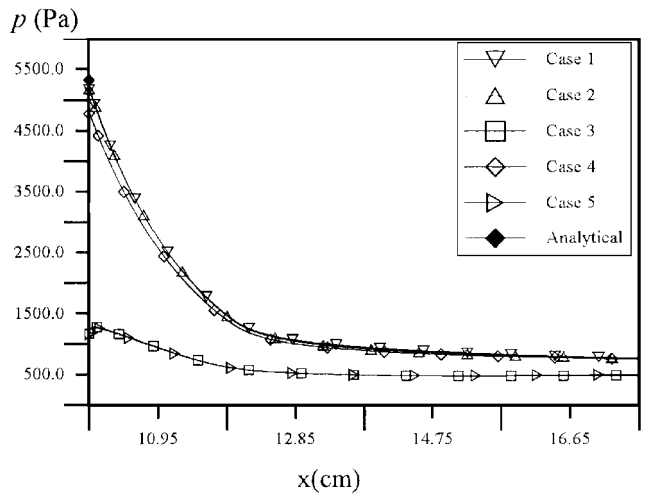

Fig. 6 Surface pressure distributions.

for case 1 because this point represents the stagnation point for the blunt body. In general, based on the flowfield plots, it is quite obvious that there are certain similarities between cases 2 and 4 and also between cases 3 and 5. Therefore, the case studies will be divided between cases 2 and 4 and between cases 3 and 5.

Cases 2 and 4

From both the contour and flowfield plots, it is clear that there is no distinction between these two cases from case 1 as far as the shock location is concerned. However, there seems to be a reduction in pressure for case 4 after the shock by about 500 Pa as compared to cases 1 and 2. Investigation of the velocity distribution suggests that the flow is symmetrical with respect to the x axis (stagnation streamline for case 1), and furthermore, there is no flow being induced in the z direction. Also the stagnation point for these two cases is the same as for case 1, which is at the nose of the blunt body. Based on the already stated arguments, it is concluded that cases 2 and 4 have their stagnation streamlines coinciding with the x axis.

Cases 3 and 5

It is apparent from the contour and pressure distribution plots that there is a considerable difference in the shock standoff distance. The results reveal that shock displacement for case 5 is comparatively much greater than that for case 3. In both cases a contact discontinuity displayed as CD in Fig. 4 is detected. Note that there is no jump in pressure across a contact discontinuity. These cases also indicate that there is a large reduction in pressure at the nose as compared to case 1. The velocity distributions indicate that the flow is no longer symmetrical with respect to the x axis and the stagnation point is no longer located on the axis of symmetry.

Figure 6 shows the surface pressure distributions for all of the cases. A reduction in pressure of about 4000 Pa at the nose region is recognized for cases 3 and 5. As for case 4, there is a pressure reduction of 500 Pa at the nose, and the reduction is almost negligible for case 2.

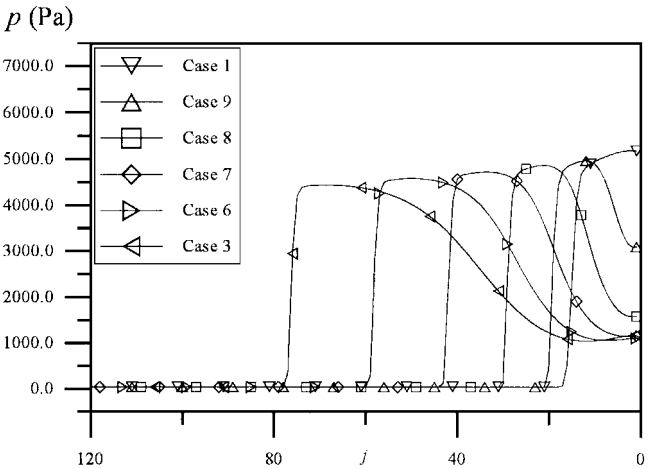

Fig. 7 Computed pressure distributions at $y = 0$ m for $B_y = 0 \rightarrow 5\sqrt{(4\pi)}$.

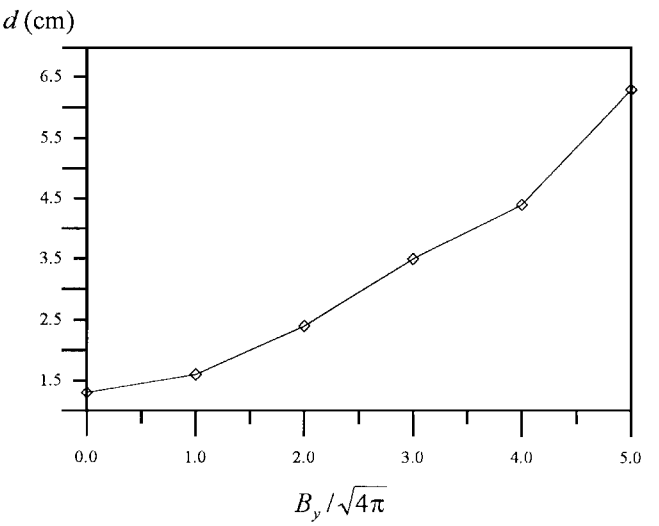

Fig. 8 Shock standoff distance at $y = 0$ m for $B_y = 0 \rightarrow 5\sqrt{(4\pi)}$.

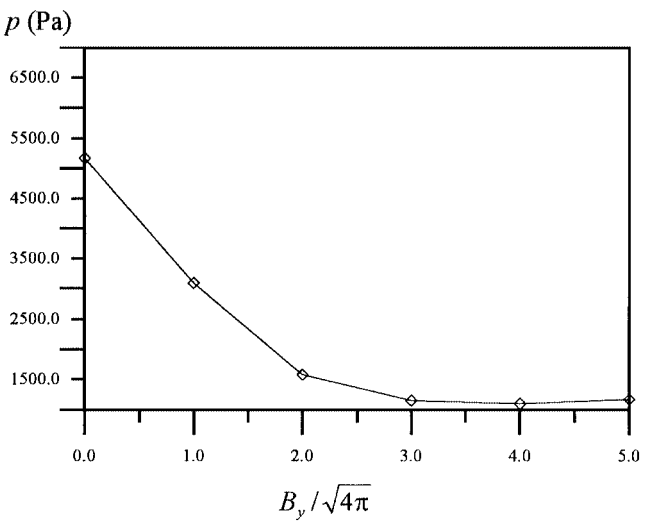

Fig. 9 Nose tip pressure for $B_y = 0 \rightarrow 5\sqrt{(4\pi)}$.

Cases 6–9

Investigation of cases 1–5 indicates that the primary component of the magnetic field that affects the flowfield is the y component. Therefore, cases 6–9 are introduced to clearly identify this effect. A comparison of shock locations as influenced by the magnetic field is shown in Figs. 7 and 8. Note that, as the value of B_y is increased,

the shock standoff distance is increased; however, this relation is not linear, as observed in Fig. 8. Furthermore, the increase in shock standoff distance is accompanied by a formation of additional flow expansion and reduction of surface pressure. The reduction of surface pressure at the blunt body nose ($y = 0$) is shown in Fig. 9. This location would be the stagnation point for the case of $\boldsymbol{B} = 0$. However, because of the asymmetry of flow introduced by the magnetic field, the location of $y = 0$ is not referred to as the stagnation point. As shown in Fig. 9, there appears to be a limiting value in the reduction of surface pressure, which is achieved at about $B_y = 3\sqrt{(4\pi)}$.

VI. Conclusions

The fourth-order modified R–K scheme augmented with the TVD model is used to solve the eight-wave structure ideal MHD in two-dimensional generalized coordinates. A set of right and inverse right eigenvectors has been developed for the implementation of the TVD model.

Several conclusions were drawn from this investigation.

1) The transverse y-component magnetic field has the tendency to displace the shock location farther away from the body while decreasing the total pressure after the shock.

2) This magnetic component creates a contact discontinuity around the nose region of the body.

3) The flowfield loses symmetricity along the symmetrical axis of the body while it displaces the stagnation point from the nose tip.

Appendix: Eigenvectors in Generalized Coordinates

The right eigenvectors of $\bar{A}$ are

$$\boldsymbol{r}_0 = \begin{bmatrix} 1 & u & v & w & 0 & 0 & 0 & \frac{1}{2}V^2 \end{bmatrix}^T \tag{A1a}$$

$$\boldsymbol{r}_{\pm v_{a\xi}} = \begin{bmatrix} 0 \\ \rho\xi_y B_z \\ -\rho\xi_x B_z \\ -\rho(\xi_y B_x - \xi_x B_y) \\ \mp\sqrt{4\pi\rho}\,\xi_y B_z \\ \pm\sqrt{4\pi\rho}\,\xi_x B_z \\ \pm\sqrt{4\pi\rho}(\xi_y B_x - \xi_x B_y) \\ \rho[\xi_x(-vB_z + wB_y) + \xi_y(uB_z - wB_x)] \end{bmatrix} \tag{A1b}$$

$$\boldsymbol{r}_{\pm v_{f\xi}} = \begin{bmatrix} \rho \\ \rho u \pm \Theta_{2\xi}/v_{f\xi}\Theta_{1\xi} \\ \rho v \pm \Theta_{3\xi}/v_{f\xi}\Theta_{1\xi} \\ \rho w \pm \Theta_{7\xi}/v_{f\xi}\Theta_{1\xi} \\ \Theta_{8\xi}/\Theta_{1\xi} \\ \Theta_{9\xi}/\Theta_{1\xi} \\ \Theta_{10\xi}/\Theta_{1\xi} \\ \left\{\frac{1}{2}\rho V^2 + \frac{1}{4}[\pm 4\pi(\gamma-1)(u\Theta_{2\xi} + v\Theta_{3\xi} + w\Theta_{7\xi}) \right. \\ \quad + v_{f\xi}(\gamma-1)(B_x\Theta_{8\xi} + B_y\Theta_{9\xi} + B_z\Theta_{10\xi}) \\ \left. \quad + 4\pi p\gamma v_{f\xi}\Theta_{1\xi}]/[(\gamma-1)\pi v_{f\xi}\Theta_{1\xi}]\right\} \end{bmatrix} \tag{A1c}$$

$$\boldsymbol{r}_{\pm v_{s\xi}} = \begin{bmatrix} \rho \\ \rho u \pm \Theta_{5\xi}/v_{s\xi}\Theta_{4\xi} \\ \rho v \pm \Theta_{6\xi}/v_{s\xi}\Theta_{4\xi} \\ \rho w \pm \Theta_{7\xi}/v_{s\xi}\Theta_{4\xi} \\ \Theta_{8\xi}/\Theta_{4\xi} \\ \Theta_{9\xi}/\Theta_{4\xi} \\ \Theta_{10\xi}/\Theta_{4\xi} \\ \left\{\frac{1}{2}\rho V^2 + \frac{1}{4}[\pm 4\pi(\gamma-1)(u\Theta_{5\xi} + v\Theta_{6\xi} + w\Theta_{7\xi}) \right. \\ \quad + v_{s\xi}(\gamma-1)(B_x\Theta_{8\xi} + B_y\Theta_{9\xi} + B_z\Theta_{10\xi}) \\ \left. \quad + 4\pi p\gamma v_{s\xi}\Theta_{4\xi}]/[(\gamma-1)\pi v_{s\xi}\Theta_{4\xi}]\right\} \end{bmatrix} \tag{A1d}$$

$$\boldsymbol{r}_{d\xi} = \begin{bmatrix} 0 & 0 & 0 & 0 & 1 & \dfrac{\xi_y}{\xi_x} & 0 & \dfrac{B_x\xi_x + B_y\xi_y}{4\pi\xi_x} \end{bmatrix}^T \tag{A1e}$$

The left (inverse right) eigenvectors are

$$\boldsymbol{l}_0 = \frac{\rho(\gamma-1)}{\gamma p} \times \begin{bmatrix} \dfrac{\gamma p}{\rho(\gamma-1)} - \dfrac{1}{2}V^2 & u & v & w & \dfrac{B_x}{4\pi} & \dfrac{B_y}{4\pi} & \dfrac{B_z}{4\pi} & -1 \end{bmatrix} \tag{A2a}$$

$$\boldsymbol{l}_{\pm v_{a\xi}} = \begin{bmatrix} -(u\Theta_{12\xi}\Theta_{7\xi} - v\Theta_{11\xi}\Theta_{7\xi} + w\Theta_{13\xi})/2\rho\Theta_{16\xi} \\ \Theta_{12\xi}\Theta_{7\xi}/2\rho\Theta_{16\xi} \\ -\Theta_{11\xi}\Theta_{7\xi}/2\rho\Theta_{16\xi} \\ \Theta_{13\xi}/2\rho\Theta_{16\xi} \\ \mp\xi_y\Theta_{10\xi}/4\sqrt{\pi\rho}\,\Theta_{17\xi} \\ \pm\xi_x\Theta_{10\xi}/4\sqrt{\pi\rho}\,\Theta_{17\xi} \\ \mp\Theta_{14\xi}/4\sqrt{\pi\rho}\,\Theta_{17\xi} \\ 0 \end{bmatrix}^T \tag{A2b}$$

$$\boldsymbol{l}_{\pm v_{f\xi}} = \begin{bmatrix} \left\{\Theta_{1\xi}[(\gamma-1)B_zV^2\Theta_{7\xi}(\xi_x\Theta_{11\xi} + \xi_y\Theta_{12\xi}) \right. \\ \quad + (\gamma-1)V^2\Theta_{13\xi}(\xi_xB_y - \xi_yB_x) \\ \quad \pm 2v_{f\xi}p\gamma\Theta_{15\xi}(\xi_xB_y - \xi_yB_x)(v\Theta_{5\xi} - u\Theta_{6\xi}) \\ \quad \mp 2v_{f\xi}p\gamma B_z\Theta_{7\xi}\Theta_{15\xi}(\xi_xu + \xi_yv) \\ \left. \quad \pm 2v_{f\xi}p\gamma B_zw\Theta_{15\xi}(\xi_x\Theta_{5\xi} + \xi_y\Theta_{6\xi})]/4p\gamma\Theta_{15\xi}\Theta_{16\xi}\right\} \\ \left\{-\Theta_{1\xi}[\mp v_{f\xi}p\gamma\Theta_{6\xi}\Theta_{15\xi}(\xi_xB_y - \xi_yB_x)_z \right. \\ \quad \mp v_{f\xi}p\gamma\Theta_{7\xi}\Theta_{15\xi}\xi_xB \\ \quad + (\gamma-1)uB_z\Theta_{7\xi}(\xi_x\Theta_{11\xi} + \xi_y\Theta_{12\xi}) \\ \left. \quad + (\gamma-1)u\Theta_{13\xi}(\xi_xB_y - \xi_yB_x)]/2p\gamma\Theta_{15\xi}\Theta_{16\xi}\right\} \\ \left\{-\Theta_{1\xi}[\pm v_{f\xi}p\gamma\Theta_{5\xi}\Theta_{15\xi}(\xi_xB_y - \xi_yB_x) \right. \\ \quad \mp v_{f\xi}p\gamma\Theta_{7\xi}\Theta_{15\xi}\xi_yB_z \\ \quad + (\gamma-1)vB_z\Theta_{7\xi}(\xi_x\Theta_{11\xi} + \xi_y\Theta_{12\xi}) \\ \left. \quad + (\gamma-1)v\Theta_{13\xi}(\xi_xB_y - \xi_yB_x)]/2p\gamma\Theta_{15\xi}\Theta_{16\xi}\right\} \\ \left\{\Theta_{1\xi}[\mp v_{f\xi}p\gamma B_z\Theta_{15\xi}(\xi_x\Theta_{5\xi} - \xi_y\Theta_{6\xi}) \right. \\ \quad - (\gamma-1)wB_z\Theta_{7\xi}(\xi_x\Theta_{11\xi} + \xi_y\Theta_{12\xi}) \\ \left. \quad - (\gamma-1)w\Theta_{13\xi}(\xi_xB_y - \xi_yB_x)]/2p\gamma\Theta_{15\xi}\xi_{16\xi}\right\} \\ \left\{-\Theta_{1\xi}[(\gamma-1)B_xB_z\left(\xi_x^2 + \xi_y^2\right)\Theta_{10\xi} \right. \\ \quad + (\gamma-1)B_x(\xi_xB_y - \xi_yB_x)\Theta_{14\xi} \\ \left. \quad - 4\pi p\gamma(\xi_xB_y - \xi_yB_x)\xi_y\Theta_{4\xi}]/8\pi p\gamma\Theta_{15\xi}\Theta_{17\xi}\right\} \\ \left\{-\Theta_{1\xi}[(\gamma-1)B_yB_z\left(\xi_x^2 + \xi_y^2\right)\Theta_{10\xi} \right. \\ \quad + (\gamma-1)B_y(\xi_xB_y - \xi_yB_x)\Theta_{14\xi} \\ \left. \quad + 4\pi p\gamma(\xi_xB_y - \xi_yB_x)\xi_x\Theta_{4\xi}]/8\pi p\gamma\Theta_{15\xi}\Theta_{17\xi}\right\} \\ \left\{-\Theta_{1\xi}B_z[(\gamma-1)B_z\left(\xi_x^2 + \xi_y^2\right)\Theta_{10\xi} \right. \\ \quad + (\gamma-1)(\xi_xB_y - \xi_yB_x)\Theta_{14\xi} \\ \left. \quad + 4\pi p\gamma\left(\xi_x^2 + \xi_y^2\right)\Theta_{4\xi}]/8\pi p\gamma\Theta_{15\xi}\Theta_{17\xi}\right\} \\ \dfrac{(\gamma-1)\Theta_{1\xi}}{2p\gamma\Theta_{15\xi}} \end{bmatrix}^T \tag{A2c}$$

$$\boldsymbol{l}_{\pm v_{s\xi}} =$$

$$\left[\begin{array}{c}
\left\{\begin{array}{l}
-\Theta_{4\xi}[(\gamma-1)B_z V^2\Theta_{7\xi}(\xi_x\Theta_{11\xi}+\xi_y\Theta_{12\xi}) \\
\quad +(\gamma-1)V^2\Theta_{13\xi}(\xi_x B_y-\xi_y B_x) \\
\quad \pm 2v_{s\xi}p\gamma\Theta_{15\xi}(\xi_x B_y-\xi_y B_x)(v\Theta_{2\xi}-u\Theta_{3\xi}) \\
\quad \mp 2v_{s\xi}p\gamma B_z\Theta_{7\xi}\Theta_{15\xi}(\xi_x u+\xi_y v) \\
\quad \pm 2v_{s\xi}p\gamma B_z w\Theta_{15\xi}(\xi_x\Theta_{2\xi}+\xi_y\Theta_{3\xi})]/4p\gamma\Theta_{15\xi}\Theta_{16\xi}
\end{array}\right\} \\
\left\{\begin{array}{l}
\Theta_{4\xi}[\mp v_{s\xi}p\gamma\Theta_{3\xi}\Theta_{15\xi}(\xi_x B_y-\xi_y B_x) \\
\quad \mp v_{s\xi}p\gamma\Theta_{7\xi}\Theta_{15\xi}\xi_x B_z \\
\quad +(\gamma-1)uB_z\Theta_{7\xi}(\xi_x\Theta_{11\xi}+\xi_y\Theta_{12\xi}) \\
\quad +(\gamma-1)u\Theta_{13\xi}(\xi_x B_y-\xi_y B_x)]/2p\gamma\Theta_{15\xi}\Theta_{16\xi}
\end{array}\right\} \\
\left\{\begin{array}{l}
\Theta_{4\xi}[\pm v_{s\xi}p\gamma\Theta_{2\xi}\Theta_{15\xi}(\xi_x B_y-\xi_y B_x) \\
\quad \mp v_{s\xi}p\gamma\Theta_{7\xi}\Theta_{15\xi}\xi_y B_z \\
\quad +(\gamma-1)vB_z\Theta_{7\xi}(\xi_x\Theta_{11\xi}+\xi_y\Theta_{12\xi}) \\
\quad +(\gamma-1)v\Theta_{13\xi}(\xi_x B_y-\xi_y B_x)]/2p\gamma\Theta_{15\xi}\Theta_{16\xi}
\end{array}\right\} \\
\left\{\begin{array}{l}
-\Theta_{4\xi}[\mp v_{s\xi}p\gamma B_z\Theta_{15\xi}(\xi_x\Theta_{2\xi}+\xi_y\Theta_{3\xi}) \\
\quad -(\gamma-1)wB_z\Theta_{7\xi}(\xi_x\Theta_{11\xi}+\xi_y\Theta_{12\xi}) \\
\quad -(\gamma-1)w\Theta_{13\xi}(\xi_x B_y-\xi_y B_x)]/2p\gamma\Theta_{15\xi}\Theta_{16\xi}
\end{array}\right\} \\
\left\{\begin{array}{l}
\Theta_{4\xi}[(\gamma-1)B_x B_z\left(\xi_x^2+\xi_y^2\right)\Theta_{10\xi} \\
\quad +(\gamma-1)B_x(\xi_x B_y-\xi_y B_x)\Theta_{14\xi} \\
\quad -4\pi p\gamma(\xi_x B_y-\xi_y B_x)\xi_y\Theta_{1\xi}]/8\pi p\gamma\Theta_{15\xi}\Theta_{17\xi}
\end{array}\right\} \\
\left\{\begin{array}{l}
\Theta_{4\xi}[(\gamma-1)B_y B_z\left(\xi_x^2+\xi_y^2\right)\Theta_{10\xi} \\
\quad +(\gamma-1)B_y(\xi_x B_y-\xi_y B_x)\Theta_{14\xi} \\
\quad +4\pi p\gamma(\xi_x B_y-\xi_y B_x)\xi_x\Theta_{1\xi}]/8\pi p\gamma\Theta_{15\xi}\Theta_{17\xi}
\end{array}\right\} \\
\left\{\begin{array}{l}
\Theta_{4\xi}B_z[(\gamma-1)B_z\left(\xi_x^2+\xi_y^2\right)\Theta_{10\xi} \\
\quad +(\gamma-1)(\xi_x B_y-\xi_y B_x)\Theta_{14\xi} \\
\quad +4\pi p\gamma\left(\xi_x^2+\xi_y^2\right)\Theta_{1\xi}]/8\pi p\gamma\Theta_{15\xi}\Theta_{17\xi}
\end{array}\right\} \\
-\dfrac{(\gamma-1)\Theta_{4\xi}}{2p\gamma\Theta_{15\xi}}
\end{array}\right]^T \tag{A2d}$$

$$\boldsymbol{l}_{d\xi} = \begin{bmatrix}
0 \\ 0 \\ 0 \\ 0 \\
\xi_x[\Theta_{9\xi}(B_y\xi_x-B_x\xi_y)+\Theta_{10\xi}B_z\xi_x]/\Theta_{17\xi} \\
\xi_x[-\Theta_{8\xi}(B_y\xi_x-B_x\xi_y)+\Theta_{10\xi}B_z\xi_y]/\Theta_{17\xi} \\
-\xi_x(\Theta_{8\xi}\xi_x+\Theta_{9\xi}\xi_y)B_z/\Theta_{17\xi} \\
0
\end{bmatrix}^T \tag{A2e}$$

where

$$\Theta_{1\xi} = 4\pi\rho v_{\xi f}^2 - \left(\xi_x^2+\xi_y^2\right)\left(B_x^2+B_y^2+B_z^2\right)$$

$$\Theta_{2\xi} = p\gamma\left[4\pi\rho v_{\xi f}^2\xi_x - B_x\left(\xi_x^2+\xi_y^2\right)(\xi_x B_x+\xi_y B_y)\right]$$

$$\Theta_{3\xi} = p\gamma\left[4\pi\rho v_{\xi f}^2\xi_y - B_y\left(\xi_x^2+\xi_y^2\right)(\xi_x B_x+\xi_y B_y)\right]$$

$$\Theta_{4\xi} = 4\pi\rho v_{\xi s}^2 - \left(\xi_x^2+\xi_y^2\right)\left(B_x^2+B_y^2+B_z^2\right)$$

$$\Theta_{5\xi} = p\gamma\left[4\pi\rho v_{\xi s}^2\xi_x - B_x\left(\xi_x^2+\xi_y^2\right)(\xi_x B_x+\xi_y B_y)\right]$$

$$\Theta_{6\xi} = p\gamma\left[4\pi\rho v_{\xi s}^2\xi_y - B_y\left(\xi_x^2+\xi_y^2\right)(\xi_x B_x+\xi_y B_y)\right]$$

$$\Theta_{7\xi} = -p\gamma\left(\xi_x^2+\xi_y^2\right)(\xi_x B_x+\xi_y B_y)B_z$$

$$\Theta_{8\xi} = -4\pi p\gamma(\xi_x B_y-\xi_y B_x)\xi_y$$

$$\Theta_{9\xi} = 4\pi p\gamma(\xi_x B_y-\xi_y B_x)\xi_x, \qquad \Theta_{10\xi} = 4\pi p\gamma\left(\xi_x^2+\xi_y^2\right)B_z$$

$$\Theta_{11\xi} = \Theta_{2\xi}-\Theta_{5\xi}, \qquad \Theta_{12\xi} = \Theta_{3\xi}-\Theta_{6\xi}$$

$$\Theta_{13\xi} = \Theta_{2\xi}\Theta_{6\xi}-\Theta_{5\xi}\Theta_{3\xi}, \qquad \Theta_{14\xi} = \xi_x\Theta_{9\xi}-\xi_y\Theta_{8\xi}$$

$$\Theta_{15\xi} = \Theta_{1\xi}-\Theta_{4\xi}$$

$$\Theta_{16\xi} = \Theta_{7\xi}B_z(\xi_x\Theta_{11\xi}+\xi_y\Theta_{12\xi})+(\xi_x B_y-\xi_y B_x)\Theta_{13\xi}$$

$$\Theta_{17\xi} = \left(\xi_x^2+\xi_y^2\right)\Theta_{10\xi}B_z+(\xi_x B_y-\xi_y B_x)\Theta_{14\xi}$$

The right and left (inverse right) eigenvectors for the flux Jacobian $\bar{B}$ matrix are obtained by substituting ξ with η in Eqs. (A1) and (A2), respectively.

Acknowledgment

This work was partially supported by the Kansas Center for Advanced Scientific Computing sponsored by the National Science Foundation EPSCoR/K*STAR Program.

References

[1]Palmer, G., "Magnetic Field Effects on the Computed Flow over a Mars Return Aerobrake," *Journal of Thermophysics and Heat Transfer*, Vol. 7, No. 2, 1993, pp. 294–301.

[2]Gombosi, T. I., Powell, K. G., and De Zeeuw, D. L., "Axisymmetric Modeling of Cometary Mass Loading on an Adaptively Refined Grid: MHD Results," *Journal of Geophysical Research*, Vol. 99, No. A11, 1994, pp. 21,525–21,539.

[3]Zachary, A. L., and Colella, P., "A Higher-Order Godunov Method for the Equations of Ideal Magnetohydrodynamics," *Journal of Computational Physics*, Vol. 99, 1992, pp. 341–347.

[4]Bell, J. B., Colella P., and Trangenstein, J. A., "High Order Godunov Methods for General Systems of Hyperbolic Conservation Laws," *Journal of Computational Physics*, Vol. 82, 1989, p. 362.

[5]Brio, M., and Wu, C. C., "An Upwind Differencing Scheme for the Equations of Ideal Magnetohydrodynamics," *Journal of Computational Physics*, Vol. 75, 1988, pp. 400–422.

[6]Dai, W., and Woodward, P. R., "Extension of the Piecewise Parabolic Method to Multidimensional Ideal Magnetohydrodynamics," *Journal of Computational Physics*, Vol. 115, 1994, pp. 485–514.

[7]Dai, W., and Woodward, P. R., "A Simple Riemann Solver and High-Order Godunov Schemes for Hyperbolic Systems of Conservation Laws," *Journal of Computational Physics*, Vol. 121, 1995, pp. 51–65.

[8]Dai, W., and Woodward, P. R., "A Second-Order Iterative Implicit-Explicit Hybrid Scheme for Hyperbolic Systems of Conservation Laws," *Journal of Computational Physics*, Vol. 128, 1996, pp. 181–196.

[9]Reddy, S., and Papadakis, M., "TVD Schemes and Their Relation to Artificial Dissipation," AIAA Paper 93-0070, Jan. 1993.

[10]Barmin, A. A., Kulikovskiy, A. G., and Pogorelov, N. V., "Shock-Capturing Approach and Nonevolutionary Solutions in Magnetohydrodynamics," *Journal of Computational Physics*, Vol. 126, 1996, pp. 77–90.

[11]Toth, G., and Odstrcil, D., "Comparison of Some Flux Corrected Transport and Total Variation Diminishing Numerical Schemes for Hydrodynamic and Magnetohydrodynamic Problems," *Journal of Computational Physics*, Vol. 128, 1996, pp. 82–100.

[12]Powell, K. G., Roe, P. L., Myong, R. S., Gombosi, T., and De Zeeuw, D., "An Upwind Scheme for Magnetohydrodynamics," AIAA Paper 95-1704, June 1995.

[13]Brackbill, J. U., and Barnes, D. C., "The Effects of Nonzero $\nabla \cdot \boldsymbol{B}$ on the Numerical Solution of the Magnetohydrodynamic Equations," *Journal of Computational Physics*, Vol. 35, 1980, pp. 426–430.

[14]Strang, G., "On the Construction and Comparison of Difference Schemes," *SIAM Journal of Numerical Analysis*, Vol. 5, 1968, p. 505.

[15]Harada, S., Augustinus, J., Hoffmann, K. A., and Agarwal, R. K. "Development of a Modified Runge–Kutta Scheme with TVD Limiters for the Ideal 1-D MHD Equations," AIAA Paper 97-2090, June 1997.

[16]Augustinus, J., Harada, S., Agarwal, R. K., and Hoffmann, K. A., "Numerical Solution of the Eight-Wave Structure Ideal MHD Equations by Modified Runge–Kutta Scheme with TVD," AIAA Paper 97-2398, June 1997.

[17]Cleary, J. W., "Effects of Angle of Attack and Bluntness on Laminar Heating-Rate Distributions of a 15° Cone at a Mach Number of 10.6," NASA TN-D-5450, Oct. 1969.

I. D. Boyd
Associate Editor